Astronomy & Astrophysics manuscript no. ms
February 1, 2013

©ESO 2013

arXiv:1301.7499v1 [astro-ph.HE] 31 Jan 2013

Synchrotron X-ray diagnostics of cutoff shape of nonthermal electron spectrum at young supernova remnants

Ryo Yamazaki[1], Yutaka Ohira[1], Makoto Sawada[1], and Aya Bamba[1]

Department of Physics and Mathematics, Aoyama Gakuin University, 5-10-1 Fuchinobe, Sagamihara 252-5258, Japan
e-mail: `ryo@phys.aoyama.ac.jp`

February 1, 2013

ABSTRACT

Context. The synchrotron X-rays can be a useful tool to investigate the electron acceleration at young supernova remnants (SNRs).
Aims. At present, since the magnetic field configuration around the shocks of SNRs is uncertain, it is not clear whether the electron acceleration is limited by SNR age, synchrotron cooling, or even escape from the acceleration region. We study if the acceleration mechanism can be constrained by the cutoff shape of the electron spectrum around the maximum energy.
Methods. We derive analytical formulae of the cutoff shape in each case where the maximum electron energy is determined by SNR age, synchrotron cooling and escape from the shock. They are related to the energy dependence of the electron diffusion coefficient. Next, we discuss whether information on the cutoff shape is provided by near future observations which gives simply the photon indices and the flux ratios in the soft and hard X-ray bands.
Results. If the power-law index of the electron spectrum is independently determined by other observations, then we can constrain the cutoff shape by comparing theoretical predictions of the photon indices and/or the flux ratios with observed data which will be measured by *NuStar* and/or *Astro-H*. Such study is helpful in understanding the acceleration mechanism. In particular, it will bring us another independent constraint on the magnetic field strength around the shocks of SNRs.

Key words. Acceleration of particles – ISM: cosmic rays – ISM: supernova remnants – Turbulence – X-rays: ISM

1. Introduction

Observations of synchrotron X-rays tell us that the young supernova remnants (SNRs) are the electron accelerator up to 10–100 TeV (e.g., Koyama et al. 1995). Spectral fitting of the synchrotron radiation from radio to X-ray bands gives us information on the acceleration mechanism. For example, the maximum energy of electrons $E_{\rm max,e}$ and the magnetic field strength B are constrained by measured roll-off frequency of the spectrum, $\nu_{\rm roll}$, which is proportional to $BE_{\rm max,e}{}^2$ (Reynolds 1998; Reynolds & Keohane 1999). Furthermore, if rapid cooling time of 1–10 yr is responsible for the observed narrow rim brightening (Vink & Laming 2003; Bamba et al. 2003, 2005a,b; Yamazaki et al. 2004) and/or time variability of the synchrotron X-rays (Uchiyama et al. 2007; Uchiyama & Aharonian 2008), then $B \sim 0.1$–1 mG is inferred, so that $E_{\rm max,e} \sim 10$ TeV. Given the values of $E_{\rm max,e}$ and B as well as the SNR age $t_{\rm age}$, we can even estimate the maximum energy of protons $E_{\rm max,p}$, which is proportional to $E_{\rm max,e}{}^2 B^2 t_{\rm age}$ (see § A.1).

For young SNRs, $\nu_{\rm roll}$ is typically below the X-ray band (e.g., Bamba et al. 2003, 2005a,b), so that synchrotron X-rays are emitted by electrons whose energy is near $E_{\rm max,e}$. Hence it is expected that information of the electron spectrum at highest energy range can be extracted from the soft and hard X-ray data. In particular, recently launched satellite *The Nuclear Spectroscopic Telescope Array (NuStar)* (Hailey et al. 2010) and near future mission *Astro-H* (Takahashi et al. 2010) will observe hard X-rays whose photon energy is larger than 10 keV. In this paper, we focus on the cutoff shape of the electron spectrum and show that it may provide another independent way to tackle the problems of particle acceleration at young SNRs (§ 2). Then, we show that observations by these satellites will play an important role in this context (§ 3 and 4).

2. Cutoff shape of electron spectrum

In this paper, we assume the shape of the electron spectrum around the maximum energy, $E_{\rm max,e}$, in the form,

$$N(E) \propto E^{-p} \exp\left[-\left(E/E_{\rm max,e}\right)^a\right] \quad . \tag{1}$$

As discussed in the following, the spectral index p and the cutoff shape parameter a contain rich information on the acceleration mechanism.

2.1. Spectral index p

When the diffusive shock acceleration works at the adiabatic shock with a compression ratio of r and the energy loss effects are negligible, the spectral index is given by $p = (r + 2)/(r - 1)$ in the test-particle limit (Bell 1978; Blandford & Ostriker 1978). In particular, $p = 2.0$ in the case of the strong shock limit $r = 4$. This simplest case may not be for actual young SNRs, in which GeV-to-TeV gamma-ray observations of youngest SNRs such as Cas A and Tycho suggest $p > 2.0$ (Abdo et al. 2010; Giordano et al. 2012). This fact has been already inferred both from radio synchrotron spectrum and from propagation model of cosmic rays from SNR to Earth (e.g., Strong & Moskalenko 1998; Putze et al. 2009; Shibata et al. 2011).

If the magnetic field is strong enough (e.g., in the Bohm diffusion model, $K(E) \propto E$, see equation (A.5)), the synchrotron cooling is responsible for a spectral break, above which the electron spectrum becomes softer and the spectral index increases by 1.0, so that $p > 3.0$ (e.g., Longair 1994). Note that sometimes the synchrotron cooling effect causes spectral hardening or pile-up (Longair 1994; Drury et al. 1999; Zirakashvili & Aharonian 2007). For typical parameters of young SNRs, however, such hard component can hardly be seen for more than a decade of electron energy. At most a small bump is formed just below $E_{\rm max,e}$, which may be seen as a small excess in the radiation spectrum (see § 4).

2.2. Cutoff shape parameter *a*

The cutoff shape parameter a also depends on the details of electron acceleration, such as the magnetic field strength and the energy dependence of the diffusion coefficient. In this paper, we assume that the diffusion coefficient of high-energy electrons in the following power-law form:

$$K(E) \propto E^{\beta} \ . \tag{2}$$

Usually the Bohm diffusion, $\beta = 1$, is widely adopted. However, in general β may deviate from unity. For example, it is well known that β becomes 1/3 if the particle diffusion is considered in the Kolmogorov magnetic turbulence, while $\beta = 1/2$ for Kraichnan turbulence (e.g., Blandford & Eichler 1987)[1]. So in these cases, the value of β even tells us the properties of magnetic turbulence. In another context, if the wave damping due to ion-neutral collisions is significant, β may approach ≈ 2 (Bykov et al. 2000; Lee et al. 2012).

In the cooling limited case, where $E_{\rm max,e}$ is determined by the balance of acceleration and synchrotron cooling ($t_{\rm acc}(E) = t_{\rm syn}(E)$), the spectral shape factor a is related to β as

$$a = \beta + 1 \ , \tag{3}$$

which is analytically derived as in § B.1. In the age-limited case, where synchrotron cooling effect is neglected and $E_{\rm max,e}$ is determined by the finite age, Kang et al. (2009) have given

$$a = 2\beta \ , \tag{4}$$

by fitting their results of numerical simulation (see also Kato & Takahara 2003). Note that in the case of Bohm diffusion (that is, $\beta = 1$), both age-limited and cooling-limited cases give the same value, $a = 2$. If $\beta \neq 1$, the values of a for the two cases are different.

It may happen that the maximum energy is limited by the escape process (Ptuskin & Zirakashvili 2005; Drury et al. 2009; Caprioli et al. 2009; Ohira et al. 2010). Here we consider the simplest case (see § B.2), in which a free escape boundary exists upstream of the shock front. In the test particle limit, we analytically derive

$$a = \beta \ . \tag{5}$$

If nonlinear effects, in particular the decay of self-excited upstream turbulence, is taken into account, then a may be slightly larger (e.g., Lee et al. 2012) although precise cutoff shape is at present highly uncertain. However, as long as $\beta \approx 1$, the escape process does not affect the maximum electron energy (Ohira et al. 2012b) and hence the cutoff shape for young SNRs.

So far, we have discussed the cutoff shape in the diffusion approximation for particle motion. Around the maximum energy, a particle mean free path tends to be longer so that the particle motion becomes ballistic (e.g., Vladimirov 2009). Our discussion could be extended to the case of superdiffusive transport, whose observational evidences have been found in interplanetary shocks (Perri & Zimbardo 2012). In such cases, cutoff shape may be modified. It is expected that the highest energy particles go out of the acceleration region more rapidly than the case of diffusive transport, so that the spectral slope may be steeper. Anyway, it can be said that cutoff shape parameter a contains rich information on the particle acceleration mechanism.

3. Synchrotron X-ray diagnostics of cutoff shape

In this section, we consider the synchrotron radiation from electrons whose energy distribution is given by equation (1). Assuming an isotropic pitch-angle distribution of electrons, the energy spectrum F_ν [erg s^{-1}cm^{-2}Hz^{-1}] of the synchrotron radiation is computed. The energy flux in the photon energy range between $\varepsilon_1 = h\nu_1$ and $\varepsilon_2 = h\nu_2$ ($\nu_1 < \nu_2$) is given by $F(\varepsilon_1 - \varepsilon_2) = \int_{\nu_1}^{\nu_2} F_\nu d\nu$. We calculate photon indices and flux ratios in various energy bands, on which we focus in the following of this paper. These spectral quantities are determined if we specify four parameters a, p, $E_{\rm max,e}$, and the magnetic field strength B in the emitting region. Note that the flux normalization is not necessary. The field strength B is only required to determine the frequency that gives the peak of the νF_ν of the synchrotron radiation, so called a roll-off frequency $\nu_{\rm roll}(\propto BE_{\rm max,e}{}^2)$, which roughly corresponds to the characteristic synchrotron frequency of electrons with $E_{\rm max,e}$ (Reynolds 1998; Reynolds & Keohane 1999). Different parameter sets but with the same value of $BE_{\rm max,e}{}^2$ give the same photon indices and the flux ratios. Therefore, independent parameters are a, p, and $BE_{\rm max,e}{}^2$.

The left panel of Figure 1 shows 10–50 keV photon index as a function of 2–10 keV photon index. We adopt $p = 2.0$ (thick lines) and 3.0 (thin lines), and $a = 0.5$ (light blue), 1 (green), 2 (red), 3 (blue) and 4 (purple). Along each line, both a and p are constant, and the quantity $BE_{\rm max,e}{}^2$ changes. In the limiting case of $BE_{\rm max,e}{}^2 \to \infty$, rolloff frequency $\nu_{\rm roll}$ goes beyond the observation band, which implies the synchrotron spectrum is well approximated by $F_\nu \propto \nu^{-(p-1)/2}$. Then the photon index becomes an asymptotic value,

$$\Gamma_\infty = \frac{p+1}{2} \ , \tag{6}$$

so that $\Gamma_\infty = 1.5$ and 2.0 for $p = 2.0$ and 3.0, respectively, which correspond to the left end of each line. When $BE_{\rm max,e}{}^2$ decreases, the rolloff frequency $\nu_{\rm roll}$ crosses the observation bands, so that the photon indices become larger than the asymptotic value Γ_∞. After passing through the harder band 10–50 keV, $\nu_{\rm roll}$ crosses the softer 2–10 keV band, so that the photon index in the former band is larger than the latter. For fixed p, if a becomes larger, the flux beyond $\nu_{\rm roll}$ more rapidly decreases, resulting larger photon index. Hence each line has steeper slope for larger a. In this paper, the value of $BE_{\rm max,e}{}^2$ is reduced to $10^3\mu$G (TeV)^2, which corresponds to the characteristic frequency of the synchrotron radiation of 2.9×10^{16} Hz. Light blue lines in all the Figures as well as the thick green line of the right panel of Figure 2 have the right end, which corresponds to this lower limit.

---

[1] In general, if the spectrum of magnetic turbulence is in a form of $E_k \propto k^{-s}$, then β and s are related as $\beta = 2 - s$ under the assumption that accelerated particles scatter via wave-particle resonance interaction. In particular, for Kolmogorov ($s = 5/3$) and Kraichnan ($s = 3/2$) turbulence, we obtain $\beta = 1/3$ and 1/2, respectively.

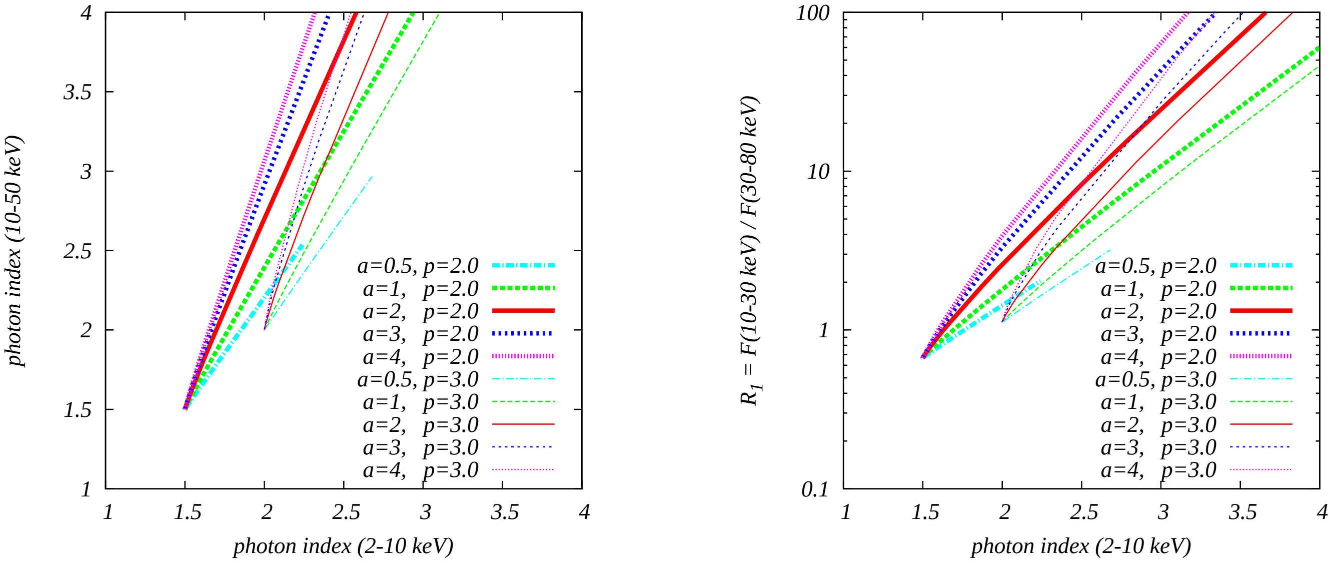

Fig. 1. Photon index in 10–50 keV band (left panel) and the flux ratio $R_1 = F(10-30\ \mathrm{keV})/F(30-80\ \mathrm{keV})$ (right panel) as functions of 2–10 keV photon index. Along each line, both a and p are constant, and the quantity $BE_{\mathrm{max,e}}{}^2$ changes from $10^3\mu\mathrm{G}\ (\mathrm{TeV})^2$ to ∞. Thick lines are for $p = 2.0$, while thin lines are for $p = 3.0$. Light blue, green, red, blue and purple lines are for $a = 0.5$, 1, 2, 3 and 4, respectively.

The right panel of Figure 1 shows the flux ratio $R_1 = F(10-30\ \mathrm{keV})/F(30-80\ \mathrm{keV})$ as a function of the 2–10 keV photon index. In the case of $BE_{\mathrm{max,e}}{}^2 \to \infty$, the hardness ratio $R = F(\varepsilon_1-\varepsilon_2)/F(\varepsilon_3-\varepsilon_4)$ of two energy bands $\varepsilon_1-\varepsilon_2$ [keV] and $\varepsilon_3-\varepsilon_4$ [keV] has an asymptotic value:

$$R \to \frac{\varepsilon_2^{2-\Gamma_\infty} - \varepsilon_1^{2-\Gamma_\infty}}{\varepsilon_4^{2-\Gamma_\infty} - \varepsilon_3^{2-\Gamma_\infty}} \ , \qquad (7)$$

for $\Gamma_\infty \neq 2$, while $R \to \ln(\varepsilon_2/\varepsilon_1)/\ln(\varepsilon_4/\varepsilon_3)$ for $\Gamma_\infty = 2$. Hence in the present case ($\varepsilon_1 = 10$ keV, $\varepsilon_2 = \varepsilon_3 = 30$ keV, and $\varepsilon_4 = 80$ keV), we have $\Gamma_\infty = 1.5$ and $R_1 \to 0.668$ for $p = 2.0$, while $\Gamma_\infty = 2.0$ and $R_1 \to 1.12$ for $p = 3.0$. When $BE_{\mathrm{max,e}}{}^2$ becomes small, both the flux ratio and the 2–10 keV photon index become large, however the decay slope is steeper for large a.

The left panel of Figure 2 shows the hardness ratio $R_2 = F(2-10\ \mathrm{keV})/F(10-80\ \mathrm{keV})$ as a function of the 2–10 keV photon index. In the limit of $BE_{\mathrm{max,e}}{}^2 \to \infty$, we have $\Gamma_\infty = 1.5$ and $R_2 \to 0.302$ for $p = 2.0$, while $\Gamma_\infty = 2.0$ and $R_2 \to 0.774$ for $p = 3.0$.

The right panel of Figure 2 shows the flux ratio $R_1 = F(10-30\ \mathrm{keV})/F(30-80\ \mathrm{keV})$ as a function of $R_3 = F(2-10\ \mathrm{keV})/F(10-30\ \mathrm{keV})$. In the limit of $BE_{\mathrm{max,e}}{}^2 \to \infty$, we have $R_1 \to 0.668$ and $R_3 \to 0.755$ for $p = 2.0$, while $R_1 \to 1.12$ and $R_3 \to 1.46$ for $p = 3.0$.

Both panels of Figure 3 are the same as Fig. 1 but for $p = 2.3$ and 3.3. The former is typical for the source spectrum of Galactic cosmic rays, which is inferred by the propagation model (e.g., Strong & Moskalenko 1998; Putze et al. 2009; Shibata et al. 2011). It is also expected from gamma-ray observations that young SNRs such as Cas A and Tycho have the energy spectrum with $p = 2.3$ (see § 4.1.2; Abdo et al. 2010). The latter case ($p = 3.3$) is realized if the synchrotron cooling is significant enough to provide a cooling break below which the electron spectrum has $p = 2.3$. In the limit of $BE_{\mathrm{max,e}}{}^2 \to \infty$, we have $\Gamma_\infty = 1.65$ and $R_1 \to 0.779$ for $p = 2.3$, while $\Gamma_\infty = 2.15$ and $R_1 \to 1.31$ for $p = 3.3$. Since differences are too small, we do not show the counterparts of Fig. 2 for $p = 2.3$ and 3.3.

4. Discussion

The value of p may be determined by the spectral slope of the radio synchrotron and/or GeV-to-TeV gamma-ray spectrum. Once p is independently determined, then comparing theoretical lines of Fig. 1 or 3 with observed data which will be provided by *NuStar* and/or *Astro-H*, we can constrain the value of a. As discussed in § 2.2, it is helpful in studying if the acceleration is age-limited, cooling-limited or escape-limited. In particular, we can check if $a \approx 2$ or not, which corresponds to the popular case of Bohm diffusion in age- or cooling-limited acceleration. One may expect that $a = 2$ is typical. Indeed, some observational results are consistent with the case of $a = 2$ (e.g., Nakamura et al. 2012), although no firm conclusion has been derived.

In addition to other observational information such as wideband radiation spectrum, X-ray spatial and temporal variability and so on, the value of a will bring us another independent constraint on the magnetic field strength (for typical example, see § 4.1.1). In another point of view, if we know, by other observations, the field strength and know how $E_{\mathrm{max,e}}$ is determined, then with the aid of Eq. (3), (4) or (5), we can further constrain the value of β, which brings us rich information on the acceleration process, in particular, the electron transport mechanism.

Note that our present method is able to constrain the value of a *without* detailed spectral fitting which needs brightness. It is easier than the spectral fitting analysis to observationally determine the flux ratios and/or photon index. Even for sources whose X-ray brightness is too small to perform the precise spectral fitting, we will be able to discuss the spectral parameter a. Hence we can obtain larger sample, which enables us to do the statistical discussion. Consequently, we will be able to extract more general properties of particle acceleration at SNRs, which cannot be done by individual analysis for the small number of bright sources.

The left panel of Fig. 2 shows that all the curves are degenerated with each other, along which the observed data points should lie if the X-ray emission arises from the synchrotron radiation. If there are outliers, we can discuss the existence of

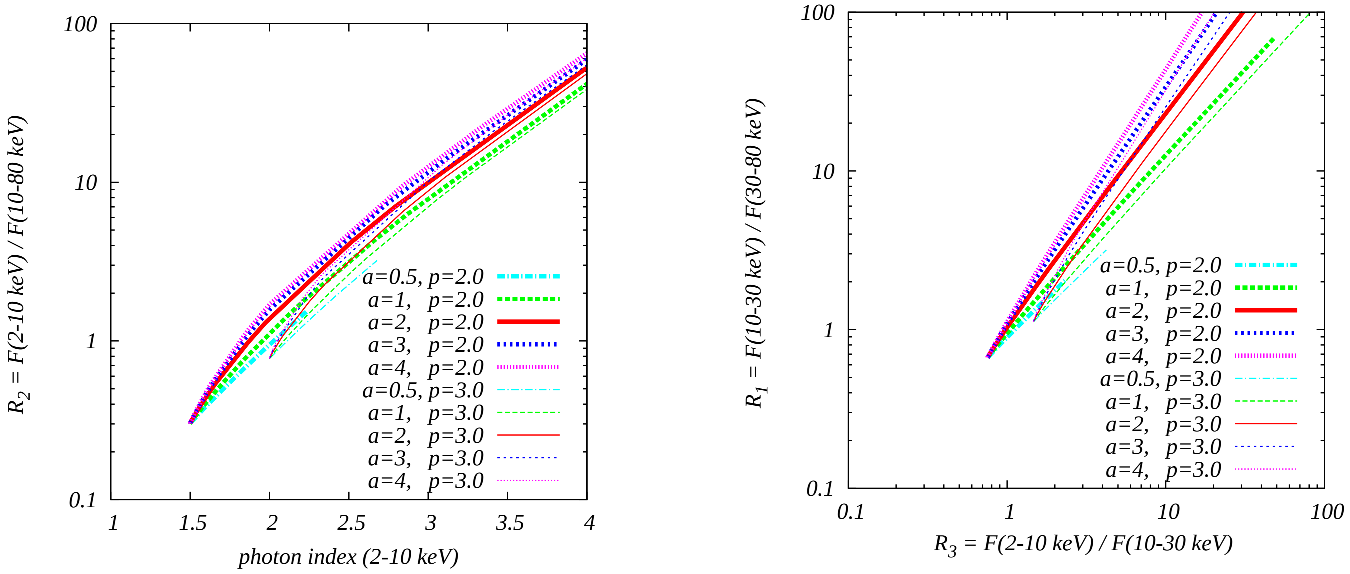

Fig. 2. The hardness ratio $R_2 = F(2-10\ \mathrm{keV})/F(10-80\ \mathrm{keV})$ as a function of the 2–10 keV photon index (left panel), and the hardness ratio $R_1 = F(10-30\ \mathrm{keV})/F(30-80\ \mathrm{keV})$ as a function of $R_3 = F(2-10\ \mathrm{keV})/F(10-30\ \mathrm{keV})$ (right panel). The meaning of each line is the same as Figure 1.

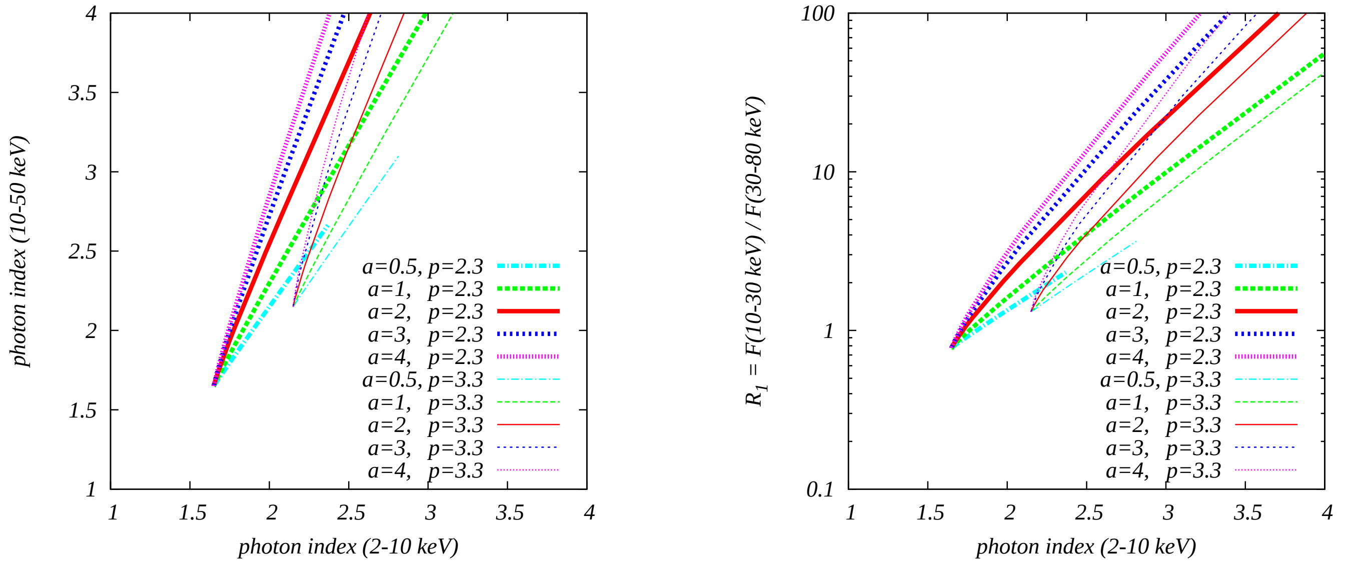

Fig. 3. The same as Fig. 1 but for $p = 2.3$ and 3.3.

extra components, such as a bump of the electron spectrum near $E_{\mathrm{max,e}}$ due to effects of pile-up via synchrotron cooling (Longair 1994; Drury et al. 1999; Zirakashvili & Aharonian 2007) and/or nonlinear acceleration (e.g., Malkov & Drury 2001), jitter or diffusive synchrotron emission (Toptygin & Fleishman 1987; Medvedev 2000; Reville & Kirk 2010; Teraki & Takahara 2011), secondary synchrotron radiation originated in accelerated protons generating charged pions (e.g., Yamazaki et al. 2006), nonthermal bremsstrahlung emission (Laming 2001a,b; Vink & Laming 2003; Vink 2008; Ohira et al. 2012a), and so on. Similar discussion may be done with the right panel of Fig. 2.

A caveat is that one-zone model is adopted for simplicity. Clearly our plots change if we see emissions from different regions which have different parameter set of B, $E_{\mathrm{max,e}}$, p, a as well as the flux normalization. In order to avoid or minimize this problem, hard X-ray observations of small emission regions are necessary. In this sense, hard X-ray imaging system onboard *NuStar* or *Astro-H* is useful.

In this paper, we have focused on hard X-rays which arise from synchrotron radiation of electrons near $E_{\mathrm{max,e}}$. It may be possible to do similar analysis in gamma-ray bands using next generation gamma-ray telescopes like CTA (Actis et al. 2011). However, at present there are several uncertainties. First, the emission mechanism is uncertain: even for representative case of SNR RX J1713.7−3946, we have not yet determined whether the gamma-ray emission is leptonic or hadronic (see § 4.1.1). Second, in the leptonic case, where the gamma-rays arise from inverse Compton emission of accelerated electrons, seed photons are uncertain; in addition to CMB, infrared and optical photons, whose intensity is uncertain and depends on the position of SNRs in the Galactic plane, significantly contribute to the gamma-ray emission. Finally, systematic error of the gamma-ray measurement might be too large for our discussion. If all of above uncertainties go out, the flux ratio and/or photon index in gamma-ray bands will be another independent diagnostics. In particular, if gamma-rays are hadronic, we can obtain the cutoff shape of protons near $E_{\rm max,p}$, which cannot be done by hard X-ray analysis proposed in this paper. However, even in this case, we need a careful analysis because spatial inhomogeneity of target matter modifies the gamma-ray spectrum (e.g., Ohira et al. 2011; Inoue et al. 2012).

4.1. Application to specific cases

In the following, let us consider the case of Cas A and RX J1713.7−3946 as representative examples.

4.1.1. RX J1713.7−3946

Tanaka et al. (2008) presented results of *Suzaku* observation of RX J1713.7−3946. XIS and HXD onboard *Suzaku* detected X-rays from this SNR in 0.4–12 keV and 12–40 keV bands, and measured photon indices in these bands are 2.39 ± 0.01 and 3.2 ± 0.1, respectively. We adopt these values as 2–10 keV and 10–50 keV photon indices, respectively. Furthermore, using the results of spectral analysis of Tanaka et al. (2008), we calculate the energy flux of the whole SNR as $F(2-10~{\rm keV}) = (4.59 \pm 0.04)\times10^{-10}{\rm erg~s^{-1}cm^{-2}}$ and $F(10-80~{\rm keV}) = (1.32\pm0.05)\times10^{-10}{\rm erg~s^{-1}cm^{-2}}$, which lead to the flux ratio, $R_2 = 3.5 \pm 0.2$. Derived value of R_2 and the adopted 2–10 keV photon index lies on theoretical lines in the left panel of Fig. 2, which implies that the X-ray emission is the synchrotron radiation.

Recently *Fermi* measured the gamma-ray spectrum of RX J1713.7−3946 in 3–300 GeV energy range, whose photon index (1.5 ± 0.1) is typical for leptonic inverse Compton emission from high-energy electrons with the spectral index $p \approx 2.0$ (Abdo et al. 2011). Hence, at first, let us consider the possibility that gamma-rays are emitted by inverse Compton scattering. Assuming CMB and infrared photons as seeds of the scattering, Li et al. (2011) extracted the electron distribution from the observed gamma-ray spectrum and obtained $p = 2.0$ and $a = 0.6$. Lee et al. (2012) also obtained similar result, $a = 0.5$, to explain the gamma-ray spectrum. The value $a = 0.6$ implies $\beta = 0.3$ in the age-limited case, while $\beta = -0.4$ in the cooling-limited case. The latter is unlikely because negative value of β is quite unnatural in the context of the magnetic turbulence. This is also inferred from the fact that the flux ratio of synchrotron X-rays to inverse Compton gamma-rays leads to the field strength $B \sim 10$–$20~\mu$G (e.g., Katz & Waxman 2008; Yamazaki et al. 2009; Ellison et al. 2010), so that synchrotron cooling effect is not significant[2]. However, one can find from Figs. 1 and 3 that no lines for $a = 0.5$ are consistent with the measured photon indices in 2–10 keV and 10–50 keV bands. In particular, $a \approx 1.5$ if $p \approx 2.0$. This fact was indicated by Tanaka et al. (2008), in which they found that the X-ray spectrum taken by *Suzaku* is consistent with both $a = 1$ and $a = 2$ cases. Therefore, the simple leptonic inverse Compton model fails to explain both the X-ray and the gamma-ray spectral shapes simultaneously.

On the other hand, hadronic scenarios for the observed hard gamma-ray spectrum are still viable if we consider the shock-cloud interaction (Inoue et al. 2012) or extreme limit of nonlinear particle acceleration (e.g., Yamazaki et al. 2009). In these cases, the strong magnetic field ($B \sim 0.1$–1 mG) is predicted, which is also inferred from the detection of time variability and narrow rim brightening of the synchrotron X-rays although there are some counter arguments (e.g., Katz & Waxman 2008; Bykov et al. 2008; Reynolds et al. 2012). Hence, the electron acceleration is limited by synchrotron cooling, so that the spectral index of electrons near $E_{\rm max,e}$ should be $p \gtrsim 3.0$ (see § 2.1). One can see from Fig. 1 that if $p \approx 3.0$, then the observed photon indices in 2–10 keV and 10–50 keV bands tells us $a \gtrsim 2$, so that $\beta \gtrsim 1$. Therefore, Bohm diffusion is consistent with observation.

Note that, however, this argument is not conclusive. We consider the spectrum of the whole SNR. As discussed previously, one-zone model may not be well. Further observations resolving smaller emission regions are necessary.

4.1.2. Cas A

XIS and HXD onboard *Suzaku* have measured the spectrum in 3.4–40 keV band (Maeda et al. 2009). They found that non-thermal component in this energy range is described by a single power-law form with a photon index of 3.06 ± 0.05. Here we adopt this value as 2-10 keV photon index, although a thermal component prevents us from determining the index precisely. Using their fitting parameter, we have $F(2-10~{\rm keV}) = (6.5\pm0.9)\times10^{-10}{\rm erg~s^{-1}cm^{-2}}$. Other observations in higher energy bands such as *Swift*/BAT (14–195 keV) (Baumgartner et al. 2012) and *BeppoSAX*/PDS (15-300 keV) (Vink & Laming 2003) show softer photon index of 3.26 ± 0.09 and 3.32 ± 0.05, respectively. Hence we expect the photon index in 10–50 keV band is slightly softer (3.1–3.3), than the value 3.06 measured by *Suzaku*. Using the parameters given by *Swift*/BAT, we have $F(10-80~{\rm keV}) = (9.6\pm0.7)\times10^{-11}{\rm erg~s^{-1}cm^{-2}}$. Then we obtain the flux ratio $R_2 \approx 6.8 \pm 1.6$.

Although the index of the electron spectrum, p, is not fixed yet, measured gamma-ray spectrum shows that p is larger than 2.0 (Abdo et al. 2010). Here we adopt $p \approx 2.3$ as a typical value. Then, one can plot the observed data in the left panels of Figures 2 and 3. Placing the observed 2–10 keV photon index of 3.06 ± 0.05 and the flux ratio $R_2 \approx 6.8 \pm 1.6$ in the left panel of Fig. 2, we find that the data is marginally consistent with theoretical prediction for the synchrotron radiation. However, the observed data point of 2–10 keV and 10–50 keV photon indices does not lie on any lines in Fig. 3. Furthermore, the observed data shows that for given value of 2–10 keV photon index, the 10–50 keV photon index is smaller than expected via the synchrotron radiation. Hence one can claim the existence of an extra component. Note that, however, this argument is based on one-zone model. At present, it is uncertain whether 2–10 keV and 10–80 keV X-rays come from the same emission region, which is left for future observations.

One may insist on explaining the observed photon indices only by the synchrotron radiation. Indeed, it is marginally possible that the observed 2–10 keV and 10–50 keV photon indices lie on the theoretical line of $p \gtrsim 3$ and $a \approx 0.5$. In this case, the acceleration is not limited by synchrotron cooling because generally $\beta > 0$ is expected (see Eq. 3). This is apparently inconsistent with the observational implications that magnetic field strength is large enough ($B \gtrsim 0.5$ mG) for the electron acceleration to be cooling limited (Vink & Laming 2003; Bamba et al. 2005a).

---

[2] There are several possibilities to explain observed time variability and narrow rim brightening of the synchrotron X-rays without amplification of the magnetic field (e.g., Katz & Waxman 2008; Bykov et al. 2008).

Acknowledgements. We would like to thank Tsunehiko Kato, Kohta Murase, Takanori Sakamoto, Atsumasa Yoshida, Tsuyoshi Inoue and Tohru Shibata for useful comments. This work was supported in part by grant-in-aid from the Ministry of Education, Culture, Sports, Science, and Technology (MEXT) of Japan, No. 24·8344 (Y. O.), No. 24840036 (M. S.) and No. 22684012 (A. B.)

References

Abdo, A. A. et al. 2010, ApJ, 710, L92
Abdo, A. A. et al. 2011, ApJ, 734, 28
Actis, M. et al. 2011, Exp. Astron., 32, 193
Bamba, A. et al. 2003, ApJ, 589, 827
Bamba, A. et al. 2005a, ApJ, 621, 793
Bamba, A. et al. 2005b, ApJ, 632, 294
Baumgartner, W. H. et al. 2012, arXiv:1212.3336
Bell, A. R. 1978, MNRAS, 182, 147
Blandford, R. D., & Ostriker, J. P., 1978, ApJ, 221, L29
Blandford, R. D., & Eichler, D., 1987, Phys. Rep., 154,1
Bykov, A. M. et al. 2000, ApJ, 538, 203
Bykov, A. M., Uvarov, Y. A., & Ellison, D. C. 2008, ApJ, 689, L133
Caprioli et al. 2009, MNRAS, 396, 2065
Drury, L. O' C., Duffy, P., Eichler, D., & Mastichiadis, A. 1999, A&A, 347, 370
Drury, L. O' C., Aharonian, F. A., Malyshev, D., & Gabici, S. 2009, A&A, 496, 1
Ellison, D. C. et al. 2010, ApJ, 712, 287
Giordano, F. et al. 2012, 744, L2
Hailey C. J. et al. 2010, in Society of Photo-Optical Instrumentation Engineers (SPIE) Conference Series, 7732, 77320T
Inoue, T. et al. 2012, ApJ, 744, 71
Kang, H., Ryu, D., & Jones, T. W. 2009, ApJ, 695, 1273
Kato, T. & Takahara, F. 2003, MNRAS, 342, 639
Katz, B., & Waxman, E. 2008, J. Cosmology Astropart. Phys., 01, 018
Koyama, K. et al. 1995, Nature, 378, 255
Laming, J. M. 2001a, ApJ, 546, 1149
Laming, J. M. 2001b, ApJ, 563, 828
Lee, S.-H. et al. 2012, 750, 156
Li, H, Liu, S., & Chen, Y. 2011, ApJ, 742, L10
Longair, M. S. 1994, High Energy Astrophysics, Vol. 2, Stars, the Galaxy and the Interstellar Medium (Cambridge: Cambridge Univ. Press)
Maeda, Y. et al. 2009, PASJ, 61, 1217
Malkov, M. A., & Drury, L. O' C. 2001, Rep. Prog. Phys., 64, 429
Medvedev, M. V. 2000, ApJ, 540, 704
Nakamura, R. et al. 2012, ApJ, 741, 134
Ohira, Y. et al. 2010, A&A, 513, A17
Ohira, Y. et al. 2011, MNRAS, 410, 1577
Ohira, Y. et al. 2012a, MNRAS, 412, L102
Ohira, Y. et al. 2012b, MNRAS, 427, 91
Perri, S. & Zimbardo, G. 2012, ApJ750, 87
Ptuskin, V. S., & Zirakashvili, V. N. 2005, A&A, 429, 755
Putze, A., Derome, L., Maurin, D., Perotto, L., & Taillet, R. 2009, A&A, 497, 991
Reville, B., Kirk, J. G., & Duffy, P. 2009, ApJ, 694, 951
Reville, B. & Kirk, J. G. 2010, ApJ, 724, 1283
Reynolds, S. P. 1998, ApJ, 493, 375
Reynolds, S. P., & Keohane, J. W. 1999, ApJ, 525, 368
Reynolds, S. P., Gaensler, B. M., & Bocchino, F. 2012, Space Science Reviews, 166, 231
Shibata, T., Ishikawa, T., & Sekiguchi, S. 2011, ApJ, 727, 38
Strong, A. W., & Moskalenko, I. V. 1998, ApJ, 509, 212
Tanaka, T. et al. 2008, ApJ, 685, 988
Takahashi, T. et al. 2010, in Society of Photo-Optical Instrumentation Engineers (SPIE) Conference Series, 7732, 77320Z
Teraki, Y. & Takahara, F. 2011, ApJ, 735, L44
Toptygin, I. N., & Fleishman, G. D. 1987, Ap&SS. 133, 213
Uchiyama, Y. et al. 2007, Nature, 449, 576
Uchiyama, Y. & Aharonian, F. A. 2008, ApJ, 677, L105
Vink, J. 2008, A&A, 486, 873
Vink, J. & Laming, J. M. 2003, ApJ, 584, 758
Vladimirov, A. 2009, Ph.D. Thesis (arXiv:0904.3760)
Yamazaki, R. et al. 2004, A&A, 416, 595
Yamazaki, R. et al. 2006, MNRAS, 371, 1975
Yamazaki, R., Kohri, K., & Katagiri, H. 2009, A&A, 495, 9
Zirakashvili, V. N. & Aharonian, F. 2007, A&A, 465, 695

Appendix A: Characteristic energies

In this section, we assume the Bohm diffusion, $K(E) \propto E$, for simplicity. More detailed analysis is found in Ohira et al. (2012b). The extension to more general case ($K(E) \propto E^{\beta}$) is easy and omitted here.

Appendix A.1: Maximum energy of accelerated electrons and protons

Let $v_{\rm s}$ and $B_{\rm d}$ be the shock velocity and the downstream magnetic field, respectively. First, suppose that the maximum energy of electrons is determined from the balance of the synchrotron loss and acceleration. Then, equating the acceleration time $t_{\rm acc}(E) = 20\xi cE/3ev_{\rm s}^2 B_{\rm d}$ with the synchrotron cooling time, $t_{\rm syn}(E) = 125~{\rm yr}(E/10~{\rm TeV})^{-1}(B_{\rm d}/100~\mu{\rm G})^{-2}$, we obtain

$$E_{\rm max}^{\rm (cool)} = \frac{24}{\xi^{1/2}}\left(\frac{v_{\rm s}}{10^8{\rm cm~s^{-1}}}\right)\left(\frac{B_{\rm d}}{10~\mu{\rm G}}\right)^{-1/2}~{\rm TeV}~, \tag{A.1}$$

where ξ is a gyro factor. On the other hand, if the cooling is not significant, the maximum energy can be determined by the condition $t_{\rm acc}(E) = t_{\rm age}$, and we obtain

$$E_{\rm max}^{\rm (age)} = \frac{4.8\times 10^2}{\xi}\left(\frac{v_{\rm s}}{10^9{\rm cm~s^{-1}}}\right)^2\left(\frac{B_{\rm d}}{10~\mu{\rm G}}\right)\left(\frac{t_{\rm age}}{10^3{\rm yr}}\right)~{\rm TeV}~. \tag{A.2}$$

For young SNRs, we typically expect the maximum energies of electrons and protons, $E_{\rm max,e}$ and $E_{\rm max,p}$ are $E_{\rm max}^{\rm (cool)}$ and $E_{\rm max}^{\rm (age)}$, respectively. Then, using equation (A.1) and (A.2), we eliminate $v_{\rm s}^2/\xi$ and obtain

$$E_{\rm max,p} \approx 83\left(\frac{E_{\rm max,e}}{10~{\rm TeV}}\right)^2\left(\frac{B_{\rm d}}{100~\mu{\rm G}}\right)^2\left(\frac{t_{\rm age}}{10^3{\rm yr}}\right)~{\rm TeV}~. \tag{A.3}$$

Appendix A.2: The cooling break energy

Let t be the characteristic time of SNR evolution, which may be the expansion time of $t_{\rm age}$ itself. Then the cooling break, $E_{\rm b}$, appears in the electron spectrum at the energy where $t_{\rm syn}(E_{\rm b}) = t$, that is,

$$E_{\rm b} = 12.5~{\rm TeV}\left(\frac{t}{10^2{\rm yr}}\right)^{-1}\left(\frac{B_{\rm d}}{100~\mu{\rm G}}\right)^{-2}~. \tag{A.4}$$

The cooling break appears if $E_{\rm b} < E_{\rm max,e} = E_{\rm max}^{\rm (cool)}$, which can be rewritten as

$$B_{\rm d} > 139~\mu{\rm G}~\xi^{1/3}\left(\frac{v_{\rm s}}{10^8{\rm cm~s^{-1}}}\right)^{-2/3}\left(\frac{t}{10^2{\rm yr}}\right)^{-2/3}~. \tag{A.5}$$

Appendix B: Analytical derivation of asymptotic spectral shape

Appendix B.1: The case of cooling-limited acceleration

Zirakashvili & Aharonian (2007) obtained the asymptotic electron spectrum near the maximum electron energy in the cooling-dominated phase, such as

$$N(E) = A_0(E)\exp\left[S_0(E)\right]~, \tag{B.1}$$

$$A_0(E) = E^{-1/2}\exp\left[\int^E \frac{\sqrt{K_2}\frac{\partial}{\partial E}\sqrt{b_2} + \sqrt{K_1}\frac{\partial}{\partial E}\sqrt{b_1}}{\sqrt{b_1 K_1} + \sqrt{b_2 K_2}}dE'\right]~,$$

(B.2)

$$S_0(E) = -\left(\frac{\gamma_s}{v_\mathrm{s}}\right)^2 \int^E \left(\frac{\sqrt{b_1K_1} + \sqrt{b_2K_2}}{E'}\right)^2 dE' \ , \tag{B.3}$$

where $\gamma_s = 3r/(r-1)$ (r is the shock compression ratio), and v_s is the shock velocity. Functions $K(E)$ and $b(E) = dE/dt$ are the diffusion coefficient and energy loss rate of electrons, respectively. Subscripts 1 and 2 indicate upstream and downstream regions of the shock, respectively. In the case of synchrotron cooling, $b(E)$ is proportional to E^2.

We assume that $K(E) = K_0E^\beta$ and $b(E) = b_0E^2$ where K_0 and b_0 are constants, and that ratios b_1/b_2 and K_1/K_2 are also constant. Then we obtain

$$A_0(E) \propto E^{1/2} \ . \tag{B.4}$$

However, for typical parameters of young SNRs, this positive slope can hardly be seen in the X-ray emission. Furthermore, neglecting non-dimensional terms on the order of unity, we derive $S_0(E) \approx -(K_0b_0/v_\mathrm{s}^2)E^{\beta+1}$. By the way, acceleration time and synchrotron cooling time are calculated as $t_\mathrm{acc}(E) \approx K_0E^\beta/v_\mathrm{s}^2$ and $t_\mathrm{syn}(E) \approx (b_0E)^{-1}$, respectively, where we again neglect terms on the order of unity. Then equating them, we obtain $E_\mathrm{max}^\mathrm{(cool)} \approx (v_\mathrm{s}^2/K_0b_0)^{1/(\beta+1)}$. Therefore, we finally derive

$$S_0(E) \approx -\left(\frac{E}{E_\mathrm{max}^\mathrm{(cool)}}\right)^{\beta+1} \ . \tag{B.5}$$

Appendix B.2: The case of escape-limited acceleration

We assume the test-particle regime and place a free escape boundary upstream at a distance of ℓ away from the shock front $x = 0$, that is, the particle distribution function is zero at $x = -\ell$ (< 0). Then stationary transport equation is solved to find a particle spectrum around the shock front given by (Caprioli et al. 2009; Reville et al. 2009)

$$N(E) \propto \exp\left\{-\frac{3r}{r-1}\int^E \frac{\mathrm{d}\log E'}{1-\exp\left[-v_\mathrm{s}\ell/K(E')\right]}\right\} \ , \tag{B.6}$$

where v_s is the shock velocity. In the escape-limited case, the maximum energy is determined by the condition (Ohira et al. 2010)

$$\frac{K(E_\mathrm{max}^\mathrm{(esc)})}{v_\mathrm{s}} = \ell \ . \tag{B.7}$$

Then, one can see $K(E)/v_\mathrm{s}\ell = K(E)/K(E_\mathrm{max}^\mathrm{(esc)}) = (E/E_\mathrm{max}^\mathrm{(esc)})^\beta$. Changing variables into $y = (E'/E_\mathrm{max}^\mathrm{(esc)})^\beta$, we derive

$$N(E) \propto \exp\left\{-\frac{3r}{r-1}\times\frac{1}{\beta}\int^{y(E)} \frac{\mathrm{d}\log y}{1-e^{-1/y}}\right\} \ , \tag{B.8}$$

where $y(E) = (E/E_\mathrm{max}^\mathrm{(esc)})^\beta$. In the case of $E \ll E_\mathrm{max}^\mathrm{(esc)}$, the term $e^{-1/y}$ can be neglected, so that we obtain $N(E) \propto E^{-3r/(r-1)}$. On the other hand, if $E \gg E_\mathrm{max}^\mathrm{(esc)}$, we approximate $1 - e^{-1/y} \approx 1/y$, resulting in $N(E) \propto \exp[-(E/E_\mathrm{max}^\mathrm{(esc)})^\beta]$, where a term on the order of unity is again neglected.